Control of Nonprehensile Planar Rolling Manipulation: A Passivity-Based Approach

Diana Serra, Fabio Ruggiero, *Member, IEEE*, Alejandro Donaire, *Member, IEEE*, Luca Rosario Buonocore, Vincenzo Lippiello, *Senior Member, IEEE*, and Bruno Siciliano, *Fellow, IEEE*

***Abstract*—This paper presents a new procedure to design a control law using the classical interconnection and damping assignment technique within the passivity-based port-Hamiltonian framework. The sought goal is to reduce the complexity of solving the so-called matching equations. The proposed approach is applied to two case studies of planar rolling nonprehensile manipulation, namely, the ball-and-beam and the eccentric disk-on-disk. The performance of the resulting controllers is illustrated through both simulations and experimental results, showing the applicability of the design in a real setup.**

***Index Terms*—Dynamic manipulation, nonprehensile rolling manipulation, passivity-based control, underactuated systems.**

I. Introduction

THE port-Hamiltonian (pH) formalism has gained the attention of the control and robotics research communities in the last decade as a methodology for modeling and control design of a complex system [1]–[5]. Rooted in the classical mechanics, the pH formalism is a representation of the system dynamics that explicitly reveals energy and physical properties related to the energy exchange, power flow, and interconnection structure. Such physical information is exploited for the design of control algorithms within nonnegligible dynamics tasks. In particular, the method of *interconnection and damping assignment passivity-based control* (IDA-PBC) is here considered [2], [5]. The IDA-PBC aims at finding a control law such that the closed loop preserves the Hamiltonian structure, with a minimum of the potential energy at the desired equilibrium, and a further damping injection to ensure asymptotic stability. The IDA-PBC method differs from other nonlinear control methodologies, typically applied in robotics, such as feedback linearization, where a linear dynamics is imposed at the expense of exact cancelation of the nonlinear system dynamics, which may cause robustness problems. The control law is then obtained by matching the open-loop and desired closed-loop dynamics. Such a match is guaranteed by solving a set of partial differential equations (PDEs), the so-called *matching equations*, which is also a bottleneck of the IDA-PBC approach despite the existence of constructive and explicit solutions for many structured problems (see, e.g., [6]–[8]).

In this paper, a new procedure to solve the matching equations for a class of mechanical systems is proposed. The carried-out approach reduces the complexity of the IDA-PBC design, while preserving its effectiveness. Under certain conditions, the proposed method consists of giving the explicit solution of a subset of PDEs resulting from the matching equations, while transforming the remaining PDEs in a set of algebraic equations. This novel procedure for the IDA-PBC design can be applied to underactuated planar mechanical systems with separable and nonseparable Hamiltonians, i.e., with constant and nonconstant mass matrices, respectively. Such a class of systems includes *nonprehensile planar rolling manipulation* tasks, which are here proposed as robotic case studies to illustrate the design procedure outlined in this paper.

Nonprehensile planar rolling manipulation systems address those tasks that involve an actuated manipulator referred to as hand and an object that is manipulated without form or force closure grasps [9]. The *disk-on-disk* [1], [10], [11], the *ball-and-beam* [12]–[15], and the *butterfly robot* [16]–[18] are some robotic benchmarks used to simulate different nonprehensile planar rolling manipulation tasks. In detail, the disk-on-disk is composed of an upper disk (object) free to roll without slipping

Manuscript received May 2, 2018; accepted November 27, 2018. Date of publication January 16, 2019; date of current version April 2, 2019. This paper was recommended for publication by Associate Editor R. Carloni and Editor T. Murphey upon evaluation of the reviewers' comments. This work was supported by the RoDyMan project, funded by the European Research Council FP7 Ideas under Advanced Grant 320992. The authors are solely responsible for the content of this paper. *(Corresponding author: Fabio Ruggiero.)*

D. Serra was with the CREATE Consortium and the Department of Electrical Engineering and Information Technology, University of Naples Federico II, 80125, Naples, Italy (e-mail: diana.serra@unina.it).

F. Ruggiero, V. Lippiello, and B. Siciliano are with the CREATE Consortium and the Department of Electrical Engineering and Information Technology, University of Naples Federico II, 80125 Naples, Italy (e-mail: fabio.ruggiero@unina.it; vincenzo.lippiello@unina.it; bruno.siciliano@unina.it).

A. Donaire is with the University of Newcastle, Callaghan, NSW 2308, Australia (e-mail: alejandro.donaire@qut.edu.au).

L. R. Buonocore is with the European Organization for Nuclear Research, 1211 Genève, Switzerland (e-mail: luca.rosario.buonocore@cern.ch).

This paper has supplementary downloadable material available at http://ieeexplore.ieee.org, provided by the author. The material consists of a video, viewable with all players supporting .mp4 format. The video shows experimental results in stabilizing the upright nonactuated disk of an eccentric disk-on-disk setup. The center of mass of the actuated disk does not coincide with the center of rotation. The underactuated setup is in full gravity, and the resulting dynamic model is with a nonseparable Hamiltonian. The proposed solution aims at reducing the complexity of solving the so-called matching equations in the classical interconnection and damping assignment technique within the passivity-based port-Hamiltonian framework. In this approach, the target potential matching equation depends on a parameterization of the desired closed-loop mass matrix. The desired energy function for the closed-loop system is selected as well. The designed solution can be applied to any underactuated mechanical system with both separable and nonseparable Hamiltonians. Contact fabio.ruggiero@unina.it for further questions about this work.

Color versions of one or more of the figures in this paper are available online at http://ieeexplore.ieee.org.

Digital Object Identifier 10.1109/TRO.2018.2887356

on the rim of a lower actuated disk (hand). The ball-and-beam consists of a beam (hand) actuated by a torque around its center of mass (CoM) together with a ball (object) rolling on it. The butterfly robot is composed of an actuated butterfly-shaped link (hand) on whose rim a ball (object) can freely roll. In all these cases, the control objective is to balance the object and drive the hand toward the desired configuration. In this paper, two nonprehensile planar rolling robotic systems with nonseparable Hamiltonian are considered as case studies: the ball-and-beam and the *eccentric disk-on-disk*. This last example is a variant of the disk-on-disk system, where the center of rotation of the hand and its geometric center are not coincident. Simulation tests on the ball-and-beam and experiments on the real physical prototype of the eccentric disk-on-disk system are presented to confirm the performance of the proposed control methodology.

The outline of this paper is as follows. Section II highlights the novelties proposed within this paper. Existing control designs for the selected case studies are described in Section III. A summary of the IDA-PBC is presented in Section IV. The main result of this paper is shown in Section V. The general dynamic model for nonprehensile planar rolling manipulation systems is derived in Section VI. The ball-and-beam and the eccentric disk-on-disk case studies are deeply analyzed in Sections VII and VIII, respectively. Section IX concludes this paper.

II. Novelties

As will be detailed in Section IV, the matching equations are split into two subsets of PDEs, namely the kinetic and the potential energy matching equations. In this paper, under certain conditions and through a suitable parameterization of the desired closed-loop mass matrix, an explicit solution is provided for the potential energy matching equation. This new procedure reduces the complexity of the IDA-PBC design by simultaneously finding the desired potential energy function for the closed-loop system and simplifying the choice of the desired mass matrix. Once the solution of the potential energy matching equation is found, the procedure to solve the kinetic energy matching equation takes inspiration from [19], without solving any PDEs.

The approach here proposed differs from [3], where the PDEs derived from the kinetic energy matching condition are transformed into a set of ordinary differential equations. Moreover, in [3] and [14], a necessary condition for the validity of the methods is that the mass matrix of the system depends only on the unactuated variable. Differently, in the proposed control approach, the open-loop mass matrix and the desired closed-loop mass matrix can be dependent on both actuated and unactuated variables.

It is worth underlining that the proposed control approach can be applied to many two-dimensional (2-D) underactuated mechanical systems having the structure outlined in Section V. Nonprehensile planar rolling manipulation systems fit into such a class. Therefore, the generalized dynamic model of nonprehensile rolling between arbitrary shapes in 2-D, presented in [20], is extended by formulating the dynamics in the pH form. Besides, the assumption that the center of actuation of the hand and its geometric center are coincident is dropped. This small technical contribution, in addition to the above-outlined control approach, overcomes the limitation in [20]. In that work, nonprehensile planar rolling manipulation systems are shown to be differentially flat only if they have a constant mass matrix (i.e., a separable Hamiltonian). The method proposed in this paper, instead, can be applied to systems having a separable Hamiltonian or a nonseparable Hamiltonian indifferently. The proposed control can be thus elected as a unifying approach to solving the stabilization problem of nonprehensile planar rolling manipulation systems. As sketched in [21], finding general strategies to settle a class of problems is yet an open issue within the nonprehensile manipulation domain.

III. Existing Control Designs for the Selected Case Studies

In the following, a brief state-of-the art about the modeling and the control of the ball-and-beam and the eccentric disk-on-disk is provided. These case studies are considered to bolster the proposed control approach. A more comprehensive analysis about nonprehensile manipulation is tackled in [21].

On the one hand, the ball-and-beam system has been extensively studied in the past years due to its peculiar feature: it fails to have a well-defined relative degree. Hence, feedback linearization cannot be applied. The authors of [13] propose an approximate input–output linearization, whereas an output feedback controller is introduced in [22]. The authors of [12] show a technique for obtaining stable and robust oscillations for such a system consisting of two steps: the former aims at finding a control law such that the closed loop of a reduced model of the dynamics is a second-order Hamiltonian system, which presents stable oscillations; in the latter step, the controller is extended to the full system using backstepping. A control method for a redundant manipulator to balance the ball-and-beam system is shown in [15]. A force/torque sensor attached to the end effector of the manipulator is used for estimating the ball position. Since it involves significant noise, a state-feedback controller is employed along with an observer.

On the other hand, the eccentric disk-on-disk has some characteristics that make it attractive as a benchmark. In [1], an IDA-PBC controller is designed ad hoc via a coordinate transformation for the traditional disk-on-disk (separable Hamiltonian), but it cannot be directly extended for the eccentric disk-on-disk (nonseparable Hamiltonian). It is worth noticing that the dynamic behavior and the stability properties of the eccentric disk-on-disk are similar to the circular ball-and-beam investigated in [23]–[25]. In [24], the Jordan form of the model of the circular ball-and-beam is linearized near the unstable equilibrium to design a linear controller. A linear control approach is also used in [23], where the limits of the beam actuator are taken into account. A geometric passivity-based control approach for this system is presented in [25]. Also, in that work, the authors propose a technique to avoid the solution of the matching conditions. Nevertheless, the gyroscopic term is not addressed for the control design within [25], since the energy shaping is applied

to a modified dynamics resulting from a geometric feedback transformation.

IV. IDA-PBC in a Nutshell

The pH framework allows modeling of mechanical systems including the information about the energy transfer explicitly. The canonical Hamiltonian equations of motion are

$$\begin{bmatrix}\dot{\boldsymbol{q}}\\ \dot{\boldsymbol{p}}\end{bmatrix} = \begin{bmatrix}\mathbf{O}_n & \boldsymbol{I}_n\\ -\boldsymbol{I}_n & \mathbf{O}_n\end{bmatrix}\nabla\mathcal{H}(\boldsymbol{q},\boldsymbol{p}) + \begin{bmatrix}\mathbf{O}_{n\times m}\\ \boldsymbol{G}(\boldsymbol{q})\end{bmatrix}\boldsymbol{u} \tag{1}$$

where $\boldsymbol{q}\in\mathbb{R}^n$ is the configuration vector, $\boldsymbol{p}\in\mathbb{R}^n$ is the momenta vector, $\boldsymbol{u}\in\mathbb{R}^m$ is the control input, $\boldsymbol{G}(\boldsymbol{q})\in\mathbb{R}^{n\times m}$ is the input mapping vector, $\boldsymbol{I}_n, \mathbf{O}_n\in\mathbb{R}^{n\times n}$ are the identity and the zero matrices, respectively, and $\mathbf{O}_{n\times m}\in\mathbb{R}^{n\times m}$ is an $n\times m$ matrix with all-zero entries. The function $\mathcal{H}:\mathbb{R}^{2n}\to\mathbb{R}$ is the Hamiltonian, which represents the total energy (kinetic plus potential) stored in the system, having the form

$$\mathcal{H}(\boldsymbol{q},\boldsymbol{p}) = \frac{1}{2}\boldsymbol{p}^T\boldsymbol{M}^{-1}(\boldsymbol{q})\boldsymbol{p} + V(\boldsymbol{q})$$

where $V(\boldsymbol{q})\in\mathbb{R}$ is the potential energy function and $\boldsymbol{M}(\boldsymbol{q}) = \boldsymbol{M}^T(\boldsymbol{q})\in\mathbb{R}^{n\times n}$ is the positive-definite mass matrix.

Stabilization of (1) to the desired equilibrium $(\boldsymbol{q},\boldsymbol{p}) = (\boldsymbol{q}^\star,\mathbf{0}_n)$, where $\mathbf{0}_n\in\mathbb{R}^n$ is the zero vector, is achieved using the IDA-PBC by assigning the target dynamics to the closed loop [14]

$$\begin{bmatrix}\dot{\boldsymbol{q}}\\ \dot{\boldsymbol{p}}\end{bmatrix} = \begin{bmatrix}\mathbf{O}_n & \boldsymbol{M}^{-1}(\boldsymbol{q})\boldsymbol{M}_d(\boldsymbol{q})\\ -\boldsymbol{M}_d(\boldsymbol{q})\boldsymbol{M}^{-1}(\boldsymbol{q}) & \boldsymbol{J}_2(\boldsymbol{q},\boldsymbol{p})\end{bmatrix}\nabla\mathcal{H}_d(\boldsymbol{q},\boldsymbol{p}) \tag{2}$$

where $\boldsymbol{J}_2(\boldsymbol{q},\boldsymbol{p})\in\mathbb{R}^{n\times n}$ is the desired interconnection matrix, and $\boldsymbol{M}_d(\boldsymbol{q})\in\mathbb{R}^{n\times n}$ is the desired mass matrix. The desired total energy function is given by

$$\mathcal{H}_d(\boldsymbol{q},\boldsymbol{p}) = \frac{1}{2}\boldsymbol{p}^T\boldsymbol{M}_d^{-1}(\boldsymbol{q})\boldsymbol{p} + V_d(\boldsymbol{q})$$

with $V_d(\boldsymbol{q})\in\mathbb{R}$ being the desired potential energy function. Then, $(\boldsymbol{q}^\star,\mathbf{0}_n)$ will be a stable equilibrium configuration of the closed loop (2) if:

C.1 $\boldsymbol{M}_d(\boldsymbol{q})$ is symmetric and positive definite;
C.2 $\boldsymbol{q}^\star = \arg\min V_d(\boldsymbol{q})$;
C.3 $\boldsymbol{J}_2(\boldsymbol{q},\boldsymbol{p})$ is skew-symmetric.

The stabilization of the desired equilibrium is achieved by identifying the class of Hamiltonian systems that can be obtained via feedback. The conditions under which this feedback law exists are the matching conditions, i.e., matching the original dynamic system (1) and the target dynamic system (2)

$$\begin{aligned}&\begin{bmatrix}\mathbf{O}_n & \boldsymbol{I}_n\\ -\boldsymbol{I}_n & \mathbf{O}_n\end{bmatrix}\nabla\mathcal{H} + \begin{bmatrix}\mathbf{O}_{n\times m}\\ \boldsymbol{G}\end{bmatrix}\boldsymbol{u}\\ &= \begin{bmatrix}\mathbf{O}_n & \boldsymbol{M}^{-1}\boldsymbol{M}_d\\ -\boldsymbol{M}_d\boldsymbol{M}^{-1} & \boldsymbol{J}_2\end{bmatrix}\nabla\mathcal{H}_d\end{aligned} \tag{3}$$

where the dependence of the functions on their argument has been dropped to simplify the notation. The first line in (3) is straightforwardly satisfied, while the second line in (3) corresponds to the following set of PDEs:

$$\begin{aligned}\boldsymbol{G}^\perp\big(&\nabla_q\mathcal{H}(\boldsymbol{q},\boldsymbol{p}) - \boldsymbol{M}_d(\boldsymbol{q})\boldsymbol{M}^{-1}(\boldsymbol{q})\nabla_q\mathcal{H}_d(\boldsymbol{q},\boldsymbol{p})\\ &+\boldsymbol{J}_2(\boldsymbol{q},\boldsymbol{p})\boldsymbol{M}_d^{-1}(\boldsymbol{q})\boldsymbol{p}\big) = 0\end{aligned} \tag{4}$$

where $\boldsymbol{G}^\perp$ is the full-rank left annihilator of $\boldsymbol{G}$. The PDEs (4) can be separated into the two subsets of PDEs as

$$\begin{aligned}\boldsymbol{G}^\perp\big(&\nabla_q(\boldsymbol{p}^T\boldsymbol{M}^{-1}(\boldsymbol{q})\boldsymbol{p}) - \boldsymbol{M}_d(\boldsymbol{q})\boldsymbol{M}^{-1}(\boldsymbol{q})\nabla_q(\boldsymbol{p}^T\boldsymbol{M}_d^{-1}(\boldsymbol{q})\boldsymbol{p})\\ &+2\boldsymbol{J}_2(\boldsymbol{q},\boldsymbol{p})\boldsymbol{M}_d^{-1}(\boldsymbol{q})\boldsymbol{p}\big) = 0\end{aligned} \tag{5}$$

$$\boldsymbol{G}^\perp\big(\nabla_q V(\boldsymbol{q}) - \boldsymbol{M}_d(\boldsymbol{q})\boldsymbol{M}^{-1}(\boldsymbol{q})\nabla_q V_d(\boldsymbol{q})\big) = 0 \tag{6}$$

where (5) and (6) are the kinetic and the potential energy matching equations, respectively. By solving (5) and (6) for $\boldsymbol{M}_d(\boldsymbol{q})$, $V_d(\boldsymbol{q})$, and $\boldsymbol{J}_2(\boldsymbol{q},\boldsymbol{p})$, subject to **C.1**–**C.3**, the energy shaping control is given by

$$\begin{aligned}\boldsymbol{u}_{es} = (\boldsymbol{G}^T\boldsymbol{G})^{-1}\boldsymbol{G}^T(&\nabla_q\mathcal{H}(\boldsymbol{q},\boldsymbol{p})\\ &- \boldsymbol{M}_d(\boldsymbol{q})\boldsymbol{M}^{-1}(\boldsymbol{q})\nabla_q\mathcal{H}_d(\boldsymbol{q},\boldsymbol{p}) + \boldsymbol{J}_2(\boldsymbol{q},\boldsymbol{p})\boldsymbol{M}_d^{-1}(\boldsymbol{q})\boldsymbol{p}).\end{aligned} \tag{7}$$

It is worth remarking that not every desired $\boldsymbol{M}_d(\boldsymbol{q})$, $V_d(\boldsymbol{q})$, and $\boldsymbol{J}_2(\boldsymbol{q},\boldsymbol{p})$ can be chosen, but only those solving (5) and (6) subject to the conditions **C.1**–**C.3**.

By applying (7) to the Hamiltonian dynamics (1), the closed-loop target dynamics (2) is obtained. Damping aimed at achieving asymptotic stability is then injected through

$$\boldsymbol{u}_{di} = -\boldsymbol{K}_v\boldsymbol{G}^T\nabla_p\mathcal{H}_d(\boldsymbol{q},\boldsymbol{p}) \tag{8}$$

where $\boldsymbol{K}_v\in\mathbb{R}^{m\times m}$ is a symmetric and positive-definite matrix. The damping injection (8) and the energy shaping control (7) are then assembled to generate the IDA-PBC

$$\boldsymbol{u} = \boldsymbol{u}_{es} + \boldsymbol{u}_{di}. \tag{9}$$

Therefore, through this adjustment, the closed-loop dynamics (2) is modified as follows:

$$\begin{bmatrix}\dot{\boldsymbol{q}}\\ \dot{\boldsymbol{p}}\end{bmatrix} = \begin{bmatrix}\mathbf{O}_n & \boldsymbol{M}^{-1}(\boldsymbol{q})\boldsymbol{M}_d(\boldsymbol{q})\\ -\boldsymbol{M}_d(\boldsymbol{q})\boldsymbol{M}^{-1}(\boldsymbol{q}) & \boldsymbol{J}_2(\boldsymbol{q},\boldsymbol{p}) - \boldsymbol{R}_d\end{bmatrix}\nabla\mathcal{H}_d(\boldsymbol{q},\boldsymbol{p}) \tag{10}$$

in which dependencies have been dropped, and $\boldsymbol{R}_d = \boldsymbol{G}\boldsymbol{K}_v\boldsymbol{G}^T\in\mathbb{R}^{n\times n}$ is the positive-(semi)definite dissipation matrix [4], [14].

V. Main Result

Consider the class of underactuated Hamiltonian systems (1) with $n=2$, $m=1$, $\boldsymbol{G} = \boldsymbol{e}_1 = \begin{bmatrix}1 & 0\end{bmatrix}^T$, and, consequently, $\boldsymbol{G}^\perp = \boldsymbol{e}_2^T = \begin{bmatrix}0 & 1\end{bmatrix}$. The first step toward the proposed resolution to solve the matching conditions is related to the potential energy PDEs and the conditions of symmetry and positive definiteness of the desired closed-loop mass matrix. Let $\boldsymbol{q} = \begin{bmatrix}q_1 & q_2\end{bmatrix}^T$ be the configuration vector, and let

$$\boldsymbol{M}(\boldsymbol{q}) = \begin{bmatrix}b_{11}(\boldsymbol{q}) & b_{12}(\boldsymbol{q})\\ b_{12}(\boldsymbol{q}) & b_{22}(\boldsymbol{q})\end{bmatrix} \tag{11}$$

be the expression of the mass matrix in (1). To look for a solution of the potential energy matching equation, the desired inertia

matrix is parameterized as follows:

$$\boldsymbol{M}_d(\boldsymbol{q},\boldsymbol{c}_1)=\Delta\begin{bmatrix}a_{11}(\boldsymbol{q},\boldsymbol{c}_1) & a_{12}(\boldsymbol{q},\boldsymbol{c}_1)\\ a_{12}(\boldsymbol{q},\boldsymbol{c}_1) & a_{22}(\boldsymbol{q},\boldsymbol{c}_1)\end{bmatrix} \tag{12}$$

where $\Delta=b_{11}(\boldsymbol{q})b_{22}(\boldsymbol{q})-b_{12}^2(\boldsymbol{q})>0$ is the determinant of $\boldsymbol{M}(\boldsymbol{q})$, and $\boldsymbol{c}_1\in\mathbb{R}^{n_{c1}}$ is a set of gains, with $n_{c1}\geq 0$, useful to design the controller. Under this assumption, the potential energy matching equation (6) becomes

$$\boldsymbol{e}_2^T\left(\nabla_q V(\boldsymbol{q})-\boldsymbol{\Gamma}(\boldsymbol{q})\nabla_q V_d(\boldsymbol{q},\boldsymbol{c}_2)\right)=0 \tag{13}$$

where $\boldsymbol{c}_2\in\mathbb{R}^{n_{c2}}$ is a set of gains, with $n_{c2}\geq 0$, useful to design the controller, and

$$\boldsymbol{\Gamma}(\boldsymbol{q},\boldsymbol{c}_1)=\begin{bmatrix}a_{11}b_{22}-a_{12}b_{12} & a_{12}b_{11}-a_{11}b_{12}\\ a_{12}b_{22}-a_{22}b_{12} & a_{22}b_{11}-a_{12}b_{12}\end{bmatrix}. \tag{14}$$

The PDE (13) can be equivalently written as

$$\nabla_{q_2}V(\boldsymbol{q})+\alpha(\boldsymbol{q})\nabla_{q_1}V_d(\boldsymbol{q},\boldsymbol{c}_2)+\beta(\boldsymbol{q})\nabla_{q_2}V_d(\boldsymbol{q},\boldsymbol{c}_2)=0 \tag{15}$$

with

$$\begin{aligned}\alpha(\boldsymbol{q},\boldsymbol{c}_1)&=a_{22}(\boldsymbol{q},\boldsymbol{c}_1)b_{12}(\boldsymbol{q})-a_{12}(\boldsymbol{q},\boldsymbol{c}_1)b_{22}(\boldsymbol{q})\\ \beta(\boldsymbol{q},\boldsymbol{c}_1)&=a_{12}(\boldsymbol{q},\boldsymbol{c}_1)b_{12}(\boldsymbol{q})-a_{22}(\boldsymbol{q},\boldsymbol{c}_1)b_{11}(\boldsymbol{q}).\end{aligned} \tag{16}$$

The main advantage of the proposed approach is the use of the scalar functions $\alpha(\boldsymbol{q},\boldsymbol{c}_1)$ and $\beta(\boldsymbol{q},\boldsymbol{c}_1)$. A suitable choice of these functions allows the possibility to have an explicit solution of (15) (see the Appendix). Notice that the form of $\alpha(\boldsymbol{q},\boldsymbol{c}_1)$ and $\beta(\boldsymbol{q},\boldsymbol{c}_1)$ and the gains $\boldsymbol{c}_1$ and $\boldsymbol{c}_2$ are selected such that $V_d(\boldsymbol{q},\boldsymbol{c}_2)$ satisfies **C.2**. Once $\alpha(\boldsymbol{q},\boldsymbol{c}_1)$, $\beta(\boldsymbol{q},\boldsymbol{c}_1)$, $\boldsymbol{c}_1$, and $\boldsymbol{c}_2$ are chosen, the terms $a_{12}(\boldsymbol{q},\boldsymbol{c}_1)$ and $a_{22}(\boldsymbol{q},\boldsymbol{c}_1)$ of the desired mass matrix are retrieved as

$$\begin{aligned}a_{12}(\boldsymbol{q}.\boldsymbol{c}_1)&=-\frac{\alpha(\boldsymbol{q},\boldsymbol{c}_1)b_{11}(\boldsymbol{q})+\beta(\boldsymbol{q},\boldsymbol{c}_1)b_{12}(\boldsymbol{q})}{\Delta}\\ a_{22}(\boldsymbol{q},\boldsymbol{c}_1)&=-\frac{\alpha(\boldsymbol{q},\boldsymbol{c}_1)b_{12}(\boldsymbol{q})+\beta(\boldsymbol{q},\boldsymbol{c}_1)b_{22}(\boldsymbol{q})}{\Delta}.\end{aligned} \tag{17}$$

Through this choice, the proposed desired closed-loop mass matrix is structurally symmetric, while condition **C.1** is fulfilled only if $a_{11}(\boldsymbol{q},\boldsymbol{c}_1)>0$ and $a_{11}(\boldsymbol{q},\boldsymbol{c}_1)a_{22}(\boldsymbol{q},\boldsymbol{c}_1)-a_{12}^2(\boldsymbol{q},\boldsymbol{c}_1)>0$. Therefore, by selecting a_{11} as

$$a_{11}(\boldsymbol{q},\boldsymbol{c}_1)=\frac{k_a a_{12}^2(\boldsymbol{q},\boldsymbol{c}_1)}{a_{22}(\boldsymbol{q},\boldsymbol{c}_1)}>0 \tag{18}$$

where $k_a>1$ is a constant parameter, the conditions for $\boldsymbol{M}_d$ to be positive definite are met if

$$\alpha(\boldsymbol{q},\boldsymbol{c}_1)b_{12}(\boldsymbol{q})+\beta(\boldsymbol{q},\boldsymbol{c}_1)b_{22}(\boldsymbol{q})<0. \tag{19}$$

Hence, the gains $\boldsymbol{c}_1$ have to be chosen to fulfill (19) without destroying the conditions found to satisfy **C.2**. If this is possible, then the desired mass matrix takes the form

$$\boldsymbol{M}_d(\boldsymbol{q})=\begin{bmatrix}-\dfrac{k_a(\alpha b_{11}+\beta b_{12})^2}{(\alpha b_{12}+\beta b_{22})} & -(\alpha b_{11}+\beta b_{12})\\ -(\alpha b_{11}+\beta b_{12}) & -(\alpha b_{12}+\beta b_{22})\end{bmatrix}. \tag{20}$$

Otherwise, it is necessary to redesign $\alpha(\boldsymbol{q},\boldsymbol{c}_1)$ and $\boldsymbol{\beta}(\boldsymbol{q},\boldsymbol{c}_1)$ and find another solution for (15).

Subsequently, the degree of freedom given by the matrix $\boldsymbol{J}_2(\boldsymbol{q},\boldsymbol{p})$ is used to satisfy the kinetic energy matching equation (5). The approach proposed in [19] is followed to deal with the kinetic energy matching equation without solving any PDE again. The interconnection matrix $\boldsymbol{J}_2$ is chosen through the following structure:

$$\boldsymbol{J}_2(\boldsymbol{q},\boldsymbol{p})=\begin{bmatrix}0 & j_2(\boldsymbol{q},\boldsymbol{p})\\ -j_2(\boldsymbol{q},\boldsymbol{p}) & 0\end{bmatrix}. \tag{21}$$

Since $\boldsymbol{e}_2^T\boldsymbol{J}_2(\boldsymbol{q},\boldsymbol{p})=-j_2(\boldsymbol{q},\boldsymbol{p})\boldsymbol{e}_1^T$, the kinetic energy matching condition (5) can be expressed as

$$\begin{aligned}&\boldsymbol{e}_2^T\nabla_q(\boldsymbol{p}^T\boldsymbol{M}^{-1}(\boldsymbol{q})\boldsymbol{p})-\boldsymbol{e}_2^T\boldsymbol{M}_d(\boldsymbol{q})\boldsymbol{M}^{-1}(\boldsymbol{q})\nabla_q(\boldsymbol{p}^T\boldsymbol{M}_d^{-1}(\boldsymbol{q})\boldsymbol{p})\\ &\quad-2j_2(\boldsymbol{q},\boldsymbol{p})\boldsymbol{e}_1^T\boldsymbol{M}_d^{-1}(\boldsymbol{q})\boldsymbol{p}=0.\end{aligned} \tag{22}$$

The scalar function $j_2(\boldsymbol{q},\boldsymbol{p})$ can be obtained solving (22) as an algebraic equation

$$\begin{aligned}j_2(\boldsymbol{q},\boldsymbol{p})=\ &\left(2\boldsymbol{e}_1^T\boldsymbol{M}_d^{-1}(\boldsymbol{q})\boldsymbol{p}\right)^{-1}\left(\boldsymbol{e}_2^T\nabla_q(\boldsymbol{p}^T\boldsymbol{M}^{-1}(\boldsymbol{q})\boldsymbol{p})\right.\\ &\left.-\boldsymbol{e}_2^T\boldsymbol{M}_d(\boldsymbol{q})\boldsymbol{M}^{-1}(\boldsymbol{q})\nabla_q(\boldsymbol{p}^T\boldsymbol{M}_d^{-1}(\boldsymbol{q})\boldsymbol{p})\right).\end{aligned} \tag{23}$$

The IDA-PBC law can be finally computed from (9). The proposed constructive solution is resumed in the flowchart depicted in Fig. 1.

The method used to satisfy the kinetic energy matching equation, inspired by [19], provides a solution that is not always well defined. Close to the equilibrium, the numerator of (23), which has a quadratic dependence on $\boldsymbol{p}$, tends toward zero faster than the denominator, which depends linearly on $\boldsymbol{p}$, thus avoiding any singularity issues. Despite this, a study about the denominator of the relation (23) reveals that, far from the equilibrium, it might be nullified if the equality $(\alpha(\boldsymbol{q},\boldsymbol{c}_1)b_{12}(\boldsymbol{q})+\beta(\boldsymbol{q},\boldsymbol{c}_1)b_{22}(\boldsymbol{q}))p_1=(\alpha(\boldsymbol{q},\boldsymbol{c}_1)b_{11}(\boldsymbol{q})+\beta(\boldsymbol{q},\boldsymbol{c}_1)b_{12}(\boldsymbol{q}))p_2$ holds, with $\boldsymbol{p}=\begin{bmatrix}p_1 & p_2\end{bmatrix}^T$. This situation is addressed in practice by saturating the denominator of (23) when its absolute value is under a small enough threshold. The simplification of the design proposed here is at the expense of the presence of possible singular solutions of (23), but these can always be numerically managed in the controller implementation.

Remark: The main result of this section can be thus applied to any underactuated mechanical system, regardless the presence of a separable Hamiltonian or a nonseparable Hamiltonian, whose dynamic model can be expressed as in (1) with $n=2$, $m=1$, and $\boldsymbol{G}=\boldsymbol{e}_1$.

VI. Dynamic Model of Nonprehensile Planar Rolling Manipulation Systems

In this section, the dynamic model of nonprehensile planar rolling systems is derived in the pH form. This formulation extends the works in [1], [11], and [20] by removing the somewhat restrictive assumption that the hand can only rotate around its CoM, which allows considering a more general class of tasks, as shown in Fig. 2. Consider the inertial world fixed frame Σ_w, which is without loss of generality attached to the holder where the hand is actuated (i.e., the center of rotation of the hand). Also, let Σ_h be the frame attached to the CoM

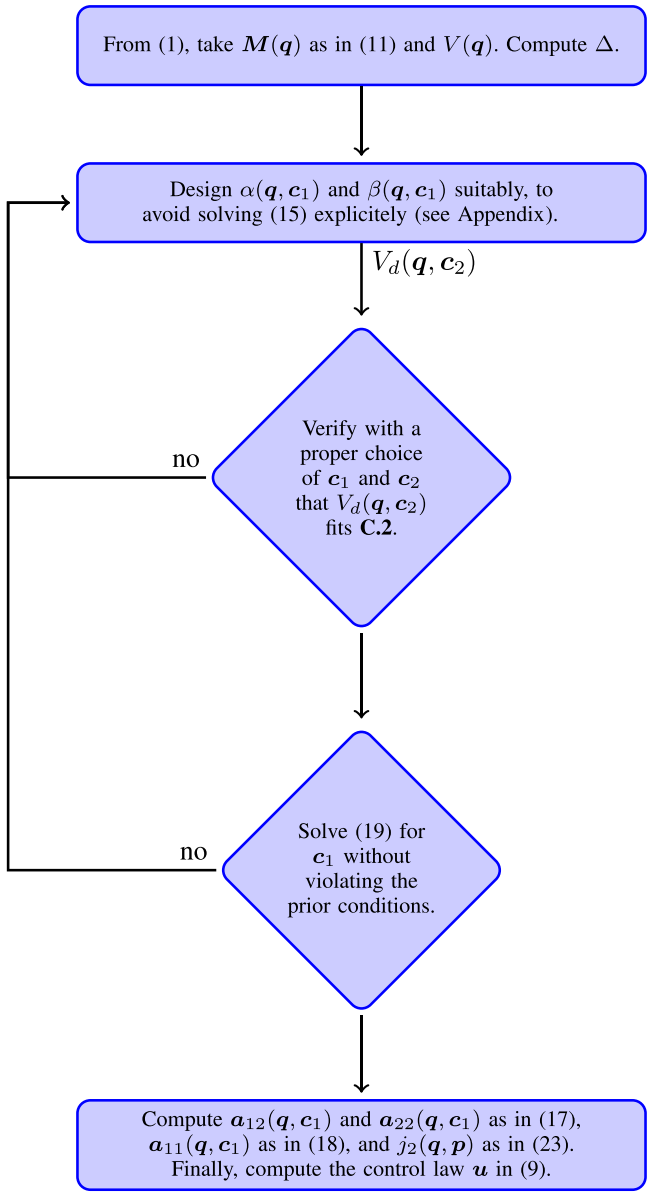

Fig. 1. Flowchart of the proposed constructive solution.

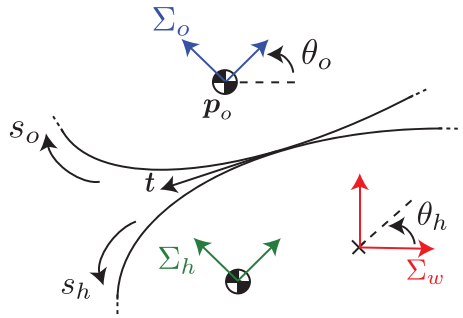

Fig. 2. General nonprehensile planar rolling manipulation system with the center of rotation of the hand (indicated by the $\times$ symbol) not corresponding to its CoM. The world fixed frame Σ_w is in red. The hand frame Σ_h and the object frame Σ_o, in green and blue, respectively, are placed at their respective centers of mass (CoMs).

of the hand, while Σ_o is the frame attached to the CoM of the object. Let $\theta_h \in \mathbb{R}$ be the angle of the hand in Σ_w, while $\boldsymbol{p}_o \in \mathbb{R}^2$ and $\theta_o \in \mathbb{R}$ are the position and the orientation, respectively, of Σ_o in Σ_w (see Fig. 2). The shapes of both the object and the hand are represented by an arclength parameterization: $s_h \in \mathbb{R}$ and $s_o \in \mathbb{R}$ are the arclength parameters for the hand and the object, respectively. At least, locally, the shapes should be of class $\mathcal{C}^2$. Any point of the hand shape is given by the chart $\boldsymbol{c}_h^h(s_h) = \begin{bmatrix} u_h(s_h) & v_h(s_h) \end{bmatrix}^T \in \mathbb{R}^2$, expressed with respect to Σ_h, while any point of the object shape is given by $\boldsymbol{c}_o^o(s_o) = \begin{bmatrix} u_o(s_o) & v_o(s_o) \end{bmatrix}^T \in \mathbb{R}^2$, expressed with respect to Σ_o. Notice that s_h increases counterclockwise along the hand, while s_o increases clockwise along the object. With this choice, the pure rolling assumption is $\dot{s}_h = \dot{s}_o$. Without loss of generality, the frames Σ_w and Σ_h coincide at $\theta_h = 0$, the point $s_h = 0$ is at the intersection between the vertical (gravitational) axis of Σ_w and the hand shape (i.e., $\boldsymbol{c}_h(0) = \begin{bmatrix} 0 & v_h(0) \end{bmatrix}^T$ in Σ_w), and thus, $s_h = s_o$ at all times during rolling. Therefore, the contact location will be specified only by s_h throughout the remainder of this paper. As the first assumption, the hand and the object maintain pure rolling contact for all time. The arclength parameterization implies the property $\|\boldsymbol{c}_h^{h\prime}\| = 1$, with the symbol $'$ indicating the derivative with respect to the parameter s_h. The same holds for $\boldsymbol{c}_o^o(s_h)$. At the contact point $\boldsymbol{c}_h^h(s_h)$, the tangent vector to the shapes is expressed as $\boldsymbol{t}^h(s_h) = \boldsymbol{c}_h^{h\prime} \in \mathbb{R}^2$ forming an angle $\phi_h(s_h) = \operatorname{atan2}(v_h'(s_h), u_h'(s_h))$ in Σ_h. The same tangent can be expressed with respect to Σ_o with an angle $\phi_o(s_h) = \operatorname{atan2}(v_o'(s_h), u_o'(s_h))$. The signed curvatures of the shapes are defined as $\kappa_h(s_h) = \phi_h'(s_h) = u_h'(s_h)v_h''(s_h) - u_h''(s_h)v_h'(s_h)$, $\kappa_o(s_h) = \phi_o'(s_h) = u_o'(s_h)v_o''(s_h) - u_o''(s_h)v_o'(s_h)$. The relative curvature at the contact point is given by

$$\kappa_r(s_h) = \kappa_h(s_h) - \kappa_o(s_h). \tag{24}$$

Notice that $\kappa_h(s_h) > 0$ and $\kappa_o(s_h) < 0$ denote convexity at the contact point for the hand and the object, respectively. Hence, $\kappa_r(s_h) > 0$ guarantees a single contact point at least locally [11]. The following constraint expresses the angle of the tangent $\boldsymbol{t}^h(s_h)$ with respect to Σ_w: $\theta_h + \phi_h(s_h) = \theta_o + \phi_o(s_h)$. Therefore, taking into account (24), the following relations hold:

$$\theta_o = \theta_h + \phi_h(s_h) - \phi_o(s_h) \tag{25a}$$

$$\dot{\theta}_o = \dot{\theta}_h + \kappa_r(s_h)\dot{s}_h. \tag{25b}$$

Assuming that $\boldsymbol{R}(\theta) \in SO(2)$ is the rotation matrix in the 2-D space, notice that the relation $\dot{\boldsymbol{R}}(\theta) = \boldsymbol{R}(\bar{\theta})\dot{\theta}$ holds with $\bar{\theta} = \theta + \frac{\pi}{2}$. The position of the CoM of the hand in Σ_w is denoted by $\boldsymbol{p}_h(\theta_h) = [\, u_w(\theta_h) \;\; v_w(\theta_h) \,]^T \in \mathbb{R}^2$. The coincidence between the contact points on both the hand and the object is expressed by $\boldsymbol{p}_h(\theta_h) + \boldsymbol{R}(\theta_h)\boldsymbol{c}_h^h(s_h) = \boldsymbol{p}_o + \boldsymbol{R}(\theta_o)\boldsymbol{c}_o^o(s_h)$, yielding to the equation $\boldsymbol{p}_o = \boldsymbol{p}_h(\theta_h) + \boldsymbol{R}(\theta_h)\boldsymbol{c}_h^h(s_h) - \boldsymbol{R}(\theta_o)\boldsymbol{c}_o^o(s_h)$, and, consequently, $\dot{\boldsymbol{p}}_o = \boldsymbol{\gamma}(\boldsymbol{q})\dot{\theta}_h + \boldsymbol{\eta}(\boldsymbol{q})\dot{s}_h = [\boldsymbol{\gamma}(\boldsymbol{q}) \;\; \boldsymbol{\eta}(\boldsymbol{q})]\dot{\boldsymbol{q}}$, with

$$\boldsymbol{\gamma} = \boldsymbol{p}_h^{\backprime} + \boldsymbol{R}(\bar{\theta}_h)\boldsymbol{c}_h^h - \boldsymbol{R}(\bar{\theta}_o)\boldsymbol{c}_o^o \tag{26a}$$

$$\boldsymbol{\eta} = \boldsymbol{R}(\theta_h)\boldsymbol{c}_h^{h\prime} - \boldsymbol{R}(\theta_o)\boldsymbol{c}_o^{o\prime} - \kappa_r\boldsymbol{R}(\bar{\theta}_o)\boldsymbol{c}_o^o \tag{26b}$$

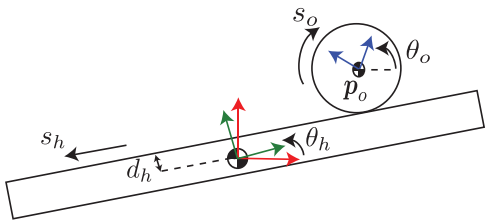

Fig. 3. Representation of the ball-and-beam system. The world fixed frame Σ_w is in red. The hand frame Σ_h and the object frame Σ_o, in green and blue, respectively, are placed at their respective CoMs.

in which dependencies have been dropped, while (25b) is included and (25a) has to be plugged in. The symbol $\backslash$ indicates the derivative with respect to θ_h, and the configuration vector is defined as $\boldsymbol{q} = [\,\theta_h \;\; s_h\,]^T$. For this class of systems, the kinetic energy is given by $T = \frac{1}{2}(I_h\dot{\theta}_h^2 + m_h\dot{\boldsymbol{p}}_h^{\mathrm{T}}(\theta_h)\dot{\boldsymbol{p}}_h(\theta_h) + m_o\dot{\boldsymbol{p}}_o^{\mathrm{T}}\dot{\boldsymbol{p}}_o + I_o\dot{\theta}_o^2) = \frac{1}{2}\boldsymbol{p}^T\boldsymbol{M}^{-1}(\boldsymbol{q})\boldsymbol{p}$, with $\boldsymbol{p} = \boldsymbol{M}(\boldsymbol{q})\dot{\boldsymbol{q}}$, and the elements of the mass matrix are given by $b_{11}(\boldsymbol{q}) = I_h + I_o + m_h\boldsymbol{p}_h^{\backslash T}\boldsymbol{p}_h^{\backslash} + m_o\boldsymbol{\gamma}^T(\boldsymbol{q})\boldsymbol{\gamma}(\boldsymbol{q})$, $b_{12}(\boldsymbol{q}) = I_o\kappa_r(s_h) + m_o\boldsymbol{\gamma}(\boldsymbol{q})^T\boldsymbol{\eta}(\boldsymbol{q})$, and $b_{22}(\boldsymbol{q}) = I_o\kappa_r^2(s_h) + m_o\boldsymbol{\eta}(\boldsymbol{q})^T\boldsymbol{\eta}(\boldsymbol{q})$. The potential energy is, instead, given by

$$V(\boldsymbol{q}) = g\boldsymbol{e}_2^T(m_o\boldsymbol{p}_o(\boldsymbol{q}) + m_h\boldsymbol{p}_h(\boldsymbol{q})). \tag{27}$$

This class of systems can be then expressed in the pH form (1), with $n = 2$, $m = 1$, and $\boldsymbol{G} = \boldsymbol{e}_1$.

VII. Case Study 1: The Ball-and-Beam

The ball-and-beam is a standard benchmark belonging to the class of nonprehensile planar rolling manipulation systems. It is composed of a ball rolling on one-degree-of-freedom linear beam. In the following, the ball-and-beam dynamic model is retrieved from the general formulation presented in Section VI. Afterwards, the procedure proposed for the IDA-PBC design is applied. Simulations are finally performed to evaluate the performance of the controller.

A. Dynamic Model of the Ball-and-Beam

The ball-and-beam system is shown in Fig. 3. It is composed of a beam that can rotate around its CoM and a ball that can only roll along the beam. The shape of the hand (i.e., the beam) is parameterized through the chart $\boldsymbol{c}_h^h(s_h) = [\,-s_h \;\; d_h\,]^T$, with $d_h \in \mathbb{R}^+$ being a fixed distance between CoM of the beam and the surface where the ball rolls. The shape of the object (i.e., the ball) is parameterized by the chart $\boldsymbol{c}_o^o(s_h) = -\rho_o[\sin\frac{s_h}{\rho_o} \;\; \cos\frac{s_h}{\rho_o}\,]^T$, with $\rho_o \in \mathbb{R}^+$ being the radius of the ball. For this system, the center of rotation of the hand corresponds to its geometric center. By considering (24), the signed curvatures of the beam and the ball are $\kappa_h = 0$ and $\kappa_o = -1/\rho_o$, respectively. The relative curvature is thus given by $\kappa_r = 1/\rho_o$. The ball's angular velocity is instead given by (25b) as $\dot{\theta}_o = \dot{\theta}_h + \dfrac{\dot{s}_h}{\rho_o}$. To compute the mass matrix of the system, the vectors $\boldsymbol{\gamma}(\boldsymbol{q})$ and $\boldsymbol{\eta}(\boldsymbol{q})$ in (26) are $\boldsymbol{\gamma}(\boldsymbol{q}) = [\,-(\rho_o + d_h)c_{\theta_h} + s_h s_{\theta_h} \;\; -(\rho_o + d_h)s_{\theta_h} - s_h c_{\theta_h}\,]^T$ and $\boldsymbol{\eta}(\boldsymbol{q}) = -[\,c_{\theta_h} \;\; s_{\theta_h}\,]^T$. The resulting elements of the mass matrix are $b_{11} = c_{b1} + c_{b2}s_h^2$, $b_{12} = \frac{I_o}{\rho_o} + m_o d_h + m_o\rho_o$, and $b_{22} = \frac{I_o}{\rho_o^2} + m_o$, where $c_{b1} = I_h + I_o + m_o d_h^2 + 2m_o d_h\rho_o + m_o\rho_o^2$ and $c_{b2} = m_o$. The potential energy (27) for this system becomes $V(\boldsymbol{q}) = m_o g[(d_h + \rho_o)\cos(\theta_h) - s_h\sin(\theta_h)]$.

In the literature, it is usual to neglect the square of s_h in $b_{11}(s_h)$. This assumption holds for slow angular rates of the beam, balls with a small mass, and short beams [13], [20], but it is not included in this paper.[1]

B. Control Design for the Ball-and-Beam

The sought goal is to stabilize the equilibrium $\boldsymbol{q}^\star = (0, s_h^\star)$, where $s_h^\star$ is the desired location of the ball on the beam. Following the procedure outlined in Section V, the quantities $\boldsymbol{M}(\boldsymbol{q})$ and $V(\boldsymbol{q})$ are retrieved from the previous subsection. The amount Δ can be thus computed. For this case study, the functions $\alpha(\boldsymbol{q}, \boldsymbol{c}_1)$ and $\beta(\boldsymbol{q}, \boldsymbol{c}_1)$ are designed as $\alpha(\theta_h, k) = k\sin(\theta_h)/\theta_h = k\mathrm{sinc}(\theta_h)$ and $\beta(\theta_h) = -\mathrm{sinc}(\theta_h)$, where $k \in \mathbb{R}$ is a gain. Notice that the $\mathrm{sinc}(\cdot)$ function is analytic everywhere. Assuming the domain of interest as $-\pi < \theta_h < \pi$, then $0 < \mathrm{sinc}(\theta_h) < 1$. Replacing the chosen functions in (15), the potential energy matching equation becomes

$$-m_o g\sin(\theta_h) + k\mathrm{sinc}(\theta_h)\nabla_{\theta_h}V_d(\boldsymbol{q}) - \mathrm{sinc}(\theta_h)\nabla_{s_h}V_d(\boldsymbol{q}) = 0. \tag{28}$$

Taking into account the results provided in the Appendix, a solution of (28) is given by

$$V_d(\boldsymbol{q}, \boldsymbol{c}_2) = \frac{m_o g\theta_h^2}{2k} + f\left(\frac{\theta_h + ks_h}{k}, \boldsymbol{c}_2\right) \tag{29}$$

where $f(\cdot)$ is a generic function of its arguments. To satisfy **C.2**, the function $f(\cdot)$ is chosen such that the desired potential function (29) results as follows:

$$V_d(\boldsymbol{q}, k_f) = \frac{m_o g\theta_h^2}{2k} - \cos\left(\frac{k_f}{k}[\theta_h + k(s_h - s_h^\star)]\right) \tag{30}$$

with $k_f \in \mathbb{R}$ a gain. To verify that $\boldsymbol{q}^\star$ is a minimum for (30), the corresponding Jacobian is first computed as

$$\nabla V_d(\boldsymbol{q}) = \begin{bmatrix} \frac{m_o g}{k}\theta_h + \frac{k_f}{k}\sin\left(\frac{k_f}{k}[\theta_h + k(s_h - s_h^\star)]\right) \\ k_f\sin\left(\frac{k_f}{k}[\theta_h + k(s_h - s_h^\star)]\right) \end{bmatrix} \tag{31}$$

where it is possible to verify that $\nabla V_d(\boldsymbol{q})$ is zero at $\boldsymbol{q}^\star$. Then, the corresponding Hessian is given by

$$\nabla^2 V_d(\boldsymbol{q}) = \begin{bmatrix} \frac{m_o g}{k} + \frac{k_f^2}{k^2}\cos\phi & \frac{k_f^2}{k}\cos\phi \\ \frac{k_f^2}{k}\cos\phi & k_f^2\cos\phi \end{bmatrix} \tag{32}$$

with $\phi = \frac{k_f}{k}(\theta_h + k(s_h - s_h^\star))$. It is possible to verify that $\nabla^2 V_d(\boldsymbol{q})$ is positive definite at the desired equilibrium $\boldsymbol{q}^\star$ if $k > 0$ and $k_f \neq 0$. Through these conditions, the desired potential function $V_d(\boldsymbol{q})$ has a minimum at the desired equilibrium $\boldsymbol{q}^\star$.

[1] It is worth noting that the model here derived is slightly different from other models addressed in the literature. For example, the model in [3] and [14] does not take into account the distance between the CoM of the beam and the surface where the ball rolls, as instead addressed by d_h in this paper.

Afterwards, inequality (19) must be solved. With the choices selected above, such an inequality becomes

$$kb_{12} - b_{22} < 0 \tag{33}$$

which has the straightforward solution $k < \frac{b_{22}}{b_{12}}$. Since it is easy to verify that $\frac{b_{22}}{b_{12}} > 0$, such a solution is not in contrast with the condition $k > 0$ necessary to make $\nabla^2 V_d(\boldsymbol{q})$ positive definite. Therefore, the gain k has to be chosen as $0 < k < \frac{b_{22}}{b_{12}}$.

Finally, the entries $a_{12}(\boldsymbol{q})$ and $a_{22}(\boldsymbol{q})$ of $\boldsymbol{M}_d(\boldsymbol{q})$ are computed, as in (17), as follows:

$$\begin{aligned} a_{12}(\boldsymbol{q}) &= -\frac{\operatorname{sinc}(\theta_h)(kb_{11}(s_h) - b_{12})}{\Delta} \\ a_{22}(\boldsymbol{q}) &= -\frac{\operatorname{sinc}(\theta_h)(kb_{12} - b_{22})}{\Delta} \end{aligned} \tag{34}$$

while $a_{11}(\boldsymbol{q})$ is taken as in (18). Therefore, the desired mass matrix is positive definite, and it can be written as follows:

$$\boldsymbol{M}_d(\boldsymbol{q}) = \begin{bmatrix} -\frac{k_a \bar{b}^2}{(kb_{12} - b_{22})} & -\operatorname{sinc}(\theta_h)\bar{b} \\ -\operatorname{sinc}(\theta_h)\bar{b} & -\operatorname{sinc}(\theta_h)(kb_{12} - b_{22}) \end{bmatrix} \tag{35}$$

with $\bar{b} = kb_{11}(s_h) - b_{12}$. The kinetic energy matching equation (5) is satisfied using (23), while the IDA-PBC control law is computed from (9).

C. Simulations of the Controlled Ball-and-Beam

Numerical tests are proposed to assess the performance of the controller for the ball-and-beam case study. The values of the parameters of the dynamic model are $m_o = 0.05$ kg, $\rho_o = 0.1$ m, $I_o = m_o\rho_o^2$, $d_h = 0.01$ m, $I_h = 0.02$ m^2·kg, and $g = 9.81$ m/s^2. The controller gains are instead chosen as $k = 4$, $k_a = 10$, $k_v = 10$, and $k_f = 1$. The sought goal is to stabilize the ball at the position $s_h^\star = 0$ m on the beam, that is, $\boldsymbol{q}^\star = (0, 0)$. Simulations are performed in the MATLAB/Simulink environment.

1) Test 1: In this first test, the chosen initial conditions are $\theta_h(0) = 0.2$ rad, $\dot{\theta}_h(0) = 0.01$ rad/s, $s_h(0) = 0$ m, and $\dot{s}_h(0) = 0$ m/s.

Fig. 4 shows the results obtained in this first simulation. In particular, the figure depicts the time histories of $\theta_h(t)$, $\dot{\theta}_h(t)$, $s_h(t)$, and $\dot{s}_h(t)$. The plots show that the controller can drive the states to the desired configuration, while demanding a sufficiently smooth control torque.

2) Test 2: In this further test, several simulations are carried out starting the ball-and-beam system from different initial configurations. The performance of the proposed controller is evaluated through the phase portrait shown in Fig. 5. In particular, the different initial conditions $(\theta_h(0), \dot{\theta}_h(0), s_h(0), \dot{s}_h(0))$ are assigned as follows: $(0.1, 0, 0.1, 0)$ in black, $(-0.1, 0, 0.1, 0)$ in blue, $(0.1, 0, -0.1, 0)$ in red, and $(-0.1, 0, -0.1, 0)$ in green. All the trajectories arrive at the origin of the phase plane, meaning that the sought goal is reached.

Besides, as an example, Fig. 6 depicts the surface of the desired potential function V_d. This exhibits a minimum at the desired equilibrium point $\boldsymbol{q}^\star$, as expected. Moreover, the red line of Fig. 6 represents the trajectory of $\theta_h(t)$ and $s_h(t)$ upon the surface of V_d when the controlled system starts at the initial condition given by $(-0.1, 0, -0.1, 0)$. The trajectory approaches the minimum of the potential energy as desired.

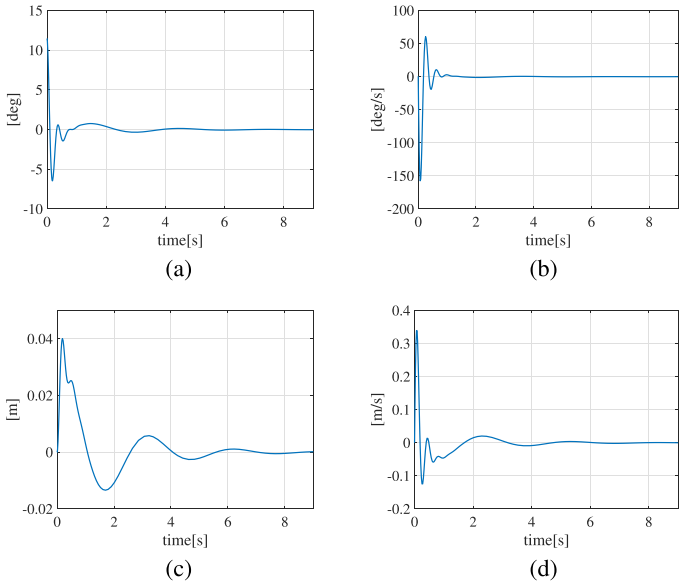

Fig. 4. Simulation test for the ball-and-beam system controlled by the proposed IDA-PBC controller. (a) Time history of $\theta_h(t)$. (b) Time history of $\dot{\theta}_h(t)$. (c) Time history of $s_h(t)$. (d) Time history of $\dot{s}_h(t)$.

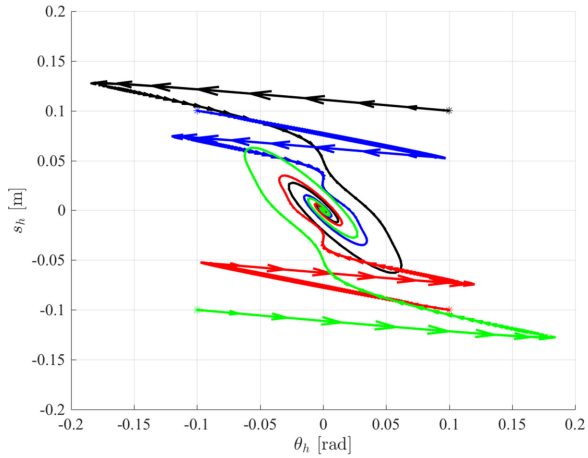

Fig. 5. Evolution of the controlled ball-and-beam system in the phase plane for different initial conditions $(\theta_h(0), \dot{\theta}_h(0), s_h(0), \dot{s}_h(0))$: $(0.1, 0, 0.1, 0)$ black line, $(-0.1, 0, 0.1, 0)$ blue line, $(0.1, 0, -0.1, 0)$ red line, and $(-0.1, 0, -0.1, 0)$ green line.

VIII. Case Study 2: The Eccentric Disk-on-Disk

The eccentric disk-on-disk system is composed of a disk freely rolling in full gravity upon a one degree of freedom actuated disk. The difference from the standard disk-on-disk system is given by the fact that the center of actuation does not coincide with the CoM. Besides, the design of a stabilizing controller for the eccentric disk-on-disk is complicated by the presence of two unstable equilibrium configurations and gyroscopic forces. In the following, the eccentric disk-on-disk dynamic model is retrieved from Section VI. Afterwards, the procedure proposed for IDA-PBC design is applied. Experiments are finally carried out.

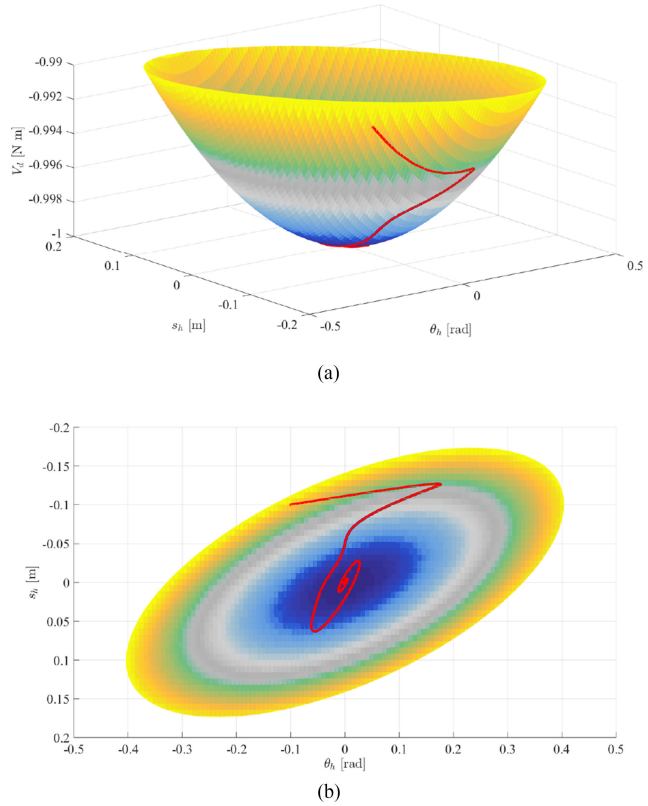

Fig. 6. Surface of the desired potential function V_d with a minimum at the desired equilibrium configuration. The red line represents the 3-D trajectory in the plane $\theta_h(t) - s_h(t)$ starting from initial conditions $(\theta_h(0), \dot{\theta}_h(0), s_h(0), \dot{s}_h(0)) = (-0.1, 0, -0.1, 0)$. (a) 3-D view of V_d. (b) 2-D view of V_d in the plane (θ_h, s_h).

A. Dynamic Model of the Eccentric Disk-on-Disk

The eccentric disk-on-disk system is represented in Fig. 7. In this system, the shape of the hand (i.e., the bottom actuated disk) is parameterized through the chart $\boldsymbol{c}_h^h(s_h) = \rho_h[-\sin\frac{s_h}{\rho_h} \cos\frac{s_h}{\rho_h}]^T$, with $\rho_h \in \mathbb{R}^+$ being the radius of the hand. The shape of the object (i.e., the top disk) is parameterized by the chart $\boldsymbol{c}_o^o(s_h) = -\rho_o[\sin\frac{s_h}{\rho_o} \cos\frac{s_h}{\rho_o}]^T$, with $\rho_o \in \mathbb{R}^+$ being the radius of the top disk. The position of the CoM of the hand in Σ_w is given by $\boldsymbol{p}_h(\theta_h) = \lambda[-s_{\theta_h} \; c_{\theta_h}]^T$, with $\lambda \in \mathbb{R}^-$ being the distance between the center of actuation and the CoM of the hand multiplied by a minus sign, and $|\lambda| < \rho_h$. By considering (24), the relative curvature is given by $\kappa_r = \frac{\rho_h + \rho_o}{\rho_h \rho_o}$. The upper disk angular velocity is given by $\dot{\theta}_o = \dot{\theta}_h + \kappa_r \dot{s}_h$. To compute the mass matrix of the system, the vectors $\boldsymbol{\gamma}(\boldsymbol{q})$ and $\boldsymbol{\eta}(\boldsymbol{q})$ are $\boldsymbol{\gamma}(\boldsymbol{q}) = -(\rho_h + \rho_o)[\cos(\theta_h + \frac{s_h}{\rho_h}) \sin(\theta_h + \frac{s_h}{\rho_h})]^T - \lambda[c_{\theta_h} \; s_{\theta_h}]^T$, and $\boldsymbol{\eta}(\boldsymbol{q}) = -\rho_o\kappa_r[\cos(\theta_h + \frac{s_h}{\rho_h}) \sin(\theta_h + \frac{s_h}{\rho_h})]^T$. Therefore, the mass matrix has the following elements: $b_{11} = c_{b1} + c_{b2}\cos(\frac{s_h}{\rho_h})$, $b_{12} = c_{b3} + c_{b4}\cos(\frac{s_h}{\rho_h})$, and $b_{22} = I_o$ $\kappa_r^2 + m_o\rho_o^2\kappa_r^2$, where $c_{b1} = I_h + I_o + \lambda^2(m_h + m_o) + m_o(\rho_h + \rho_o)^2$, $c_{b2} = 2\lambda m_o(\rho_h + \rho_o)$, $c_{b3} = I_o\kappa_r + m_o\frac{(\rho_h+\rho_o)^2}{\rho_h}$, and $c_{b4} = m_o\lambda\rho_o\kappa_r$. The potential energy (27) for the eccentric disk-on-disk is given by $V(\boldsymbol{q}) = g(m_o(\rho_h + \rho_o)\cos(\theta_h + \frac{s_h}{\rho_h}) + (m_o + m_h)\lambda\cos(\theta_h))$.

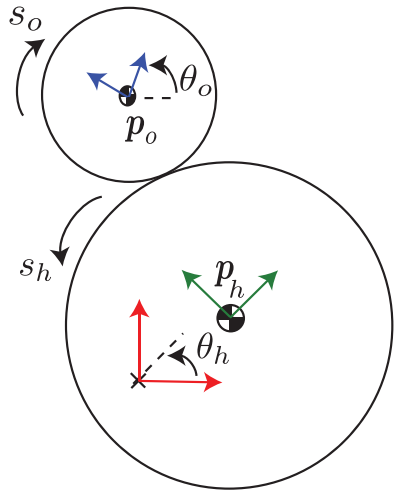

Fig. 7. Representation of the eccentric disk-on-disk system is shown in this figure. The center of rotation of the hand (indicated by the $\times$ symbol) does not correspond to its CoM. The world fixed frame Σ_w is shown in red. The hand frame Σ_h is represented in green, while the object frame Σ_o is represented in blue. Σ_h and Σ_o are placed at the respective CoMs.

B. Control Design for the Eccentric Disk-on-Disk

The sought goal is to balance the upper disk at the upright position of the hand. In this configuration, the bottom disk can present its CoM both above and below its center of actuation. With a proper change of coordinates, it is possible to express the desired equilibrium point as $\boldsymbol{q}^\star = (0, 0)$ in both cases.

Following Section V, the quantities $\boldsymbol{M}(\boldsymbol{q})$ and $V(\boldsymbol{q})$ are retrieved from the previous subsection. The amount Δ can be thus computed. The functions $\alpha(\boldsymbol{q}, \boldsymbol{c}_1)$ and $\beta(\boldsymbol{q}, \boldsymbol{c}_1)$ are designed as $\alpha(\theta_h, s_h) = \text{sinc}(\theta_h + \frac{s_h}{\rho_h})$ and $\beta(\theta_h, s_h, k) = k\text{sinc}(\theta_h + \frac{s_h}{\rho_h})$, where $k \in \mathbb{R}$ is a gain. Assuming the domain of interest as $-\pi < (\theta_h + \frac{s_h}{\rho_h}) < \pi$, then $0 < \text{sinc}(\theta_h + \frac{s_h}{\rho_h}) < 1$. Replacing the chosen functions in (15) yields

$$-c_v \sin\left(\theta_h + \frac{s_h}{\rho_h}\right) + \text{sinc}\left(\theta_h + \frac{s_h}{\rho_h}\right)\nabla_{\theta_h} V_d(\boldsymbol{q}) + k\text{sinc}\left(\theta_h + \frac{s_h}{\rho_h}\right)\nabla_{s_h} V_d(\boldsymbol{q}) = 0 \tag{36}$$

where $c_v = m_o g\frac{\rho_h + \rho_o}{\rho_h}$ is a positive parameter. Taking into account the results provided in the Appendix, a solution of (36) is given by

$$V_d(\boldsymbol{q}, \boldsymbol{c}_2) = \frac{c_v\theta_h^2(\rho_h - k) + 2c_v\theta_h s_h}{2\rho_h} + f(s_h - k\theta_h, \boldsymbol{c}_2) \tag{37}$$

where $f(\cdot)$ is a generic function of its arguments. To satisfy **C**.2, $f(\cdot)$ is chosen such that (37) becomes

$$V_d(\boldsymbol{q}, k_f) = \frac{c_v\theta_h^2(\rho_h - k) + 2c_v\theta_h s_h}{2\rho_h} + k_f(s_h - k\theta_h)^2 \tag{38}$$

where $k_f \in \mathbb{R}$ is a gain. To verify that $\boldsymbol{q}^\star$ is a minimum for (38), the corresponding Jacobian is first computed as

$$\nabla V_d(\boldsymbol{q}) = \begin{bmatrix} \frac{c_v(-k\theta_h+\theta_h\rho_h+s_h)}{\rho_h} + 2kk_f(k\theta_h - s_h) \\ \frac{c_v\theta_h}{\rho_h} - 2kk_f\theta_h + 2k_f s_h \end{bmatrix} \quad (39)$$

where it is possible to verify that $\nabla V_d(\boldsymbol{q})$ is zero at $\boldsymbol{q}^\star$. Then, the corresponding Hessian is given by

$$\nabla^2 V_d(\boldsymbol{q}) = \begin{bmatrix} c_v + 2k^2k_f - \frac{c_v k}{\rho_h} & -2kk_f + \frac{c_v}{\rho_h} \\ -2kk_f + \frac{c_v}{\rho_h} & 2k_f \end{bmatrix}. \quad (40)$$

It is possible to verify that $\nabla^2 V_d(\boldsymbol{q})$ is positive definite at the desired equilibrium $\boldsymbol{q}^\star$ if $k > -\rho_h$ and $k_f > \frac{c_v}{2\rho_h(k+\rho_h)}$ Through these conditions, $V_d(\boldsymbol{q})$ has a minimum at the desired equilibrium $\boldsymbol{q}^\star$.

Afterwards, inequality (19) must be solved. With the choices selected above, such an inequality becomes

$$b_{12}(s_h) + kb_{22} < 0 \quad (41)$$

which has the straightforward solution $k < -\frac{b_{12}(s_h)}{b_{22}}$. Since it is possible to verify that $\rho_h > \frac{(c_{b3}-c_{b4})}{b_{22}}$, such a solution is not in contrast with the condition $k > -\rho_h$ necessary to make $\nabla^2 V_d(\boldsymbol{q})$ positive definite. Therefore, the gain k must be chosen as $-\rho_h < k < -\frac{c_{b3}-c_{b4}}{b_{22}}$.

Finally, the entries $a_{12}(\boldsymbol{q})$ and $a_{22}(\boldsymbol{q})$ of $\boldsymbol{M}_d(\boldsymbol{q})$ are computed as in (17), as follows:

$$\begin{aligned} a_{12}(\boldsymbol{q}) &= -\frac{\operatorname{sinc}\left(\theta_h + \frac{s_h}{\rho_h}\right)(b_{11}(s_h) + kb_{12}(s_h))}{\Delta} \\ a_{22}(\boldsymbol{q}) &= -\frac{\operatorname{sinc}\left(\theta_h + \frac{s_h}{\rho_h}\right)(b_{12}(s_h) + kb_{22})}{\Delta} \end{aligned} \quad (42)$$

while $a_{11}(\boldsymbol{q})$ is taken as in (18). The desired mass matrix is thus positive definite, and it can be written as follows:

$$\boldsymbol{M}_d(\boldsymbol{q}) = \begin{bmatrix} \Delta a_{11} & -h_s(b_{11}+kb_{12}) \\ -h_s(b_{11}+kb_{12}) & -h_s(b_{12}+kb_{22}) \end{bmatrix} \quad (43)$$

where $h_s(\boldsymbol{q}) = \operatorname{sinc}(\theta_h + \frac{s_h}{\rho_h})$. The kinetic energy matching equation (5) is satisfied using (23), while the IDA-PBC control law is computed from (9).

C. Experiments on the Eccentric Disk-on-Disk

The performance of the proposed IDA-PBC controller is evaluated on the experimental eccentric disk-on-disk setup shown in Fig. 8(a). The lower disk (i.e., the hand) is actuated by a DC Minertia R01SA motor, able to give a peak torque of 0.54 N·m and mounting an RSD-14B Harmonic Drive model whose gearhead ratio is 50:1. With this configuration, it is possible to reach a continuous torque of 5.5 N·m with a maximum peak of 27 N·m, while the position accuracy is of about 13 arcsec. The rotation axis of the motor is placed at a distance $|\lambda| = 0.04$ m from the geometric center of the hand, as shown in Fig. 8(b). The lower disk is homogeneous, and then, the geometric center coincides with its CoM.

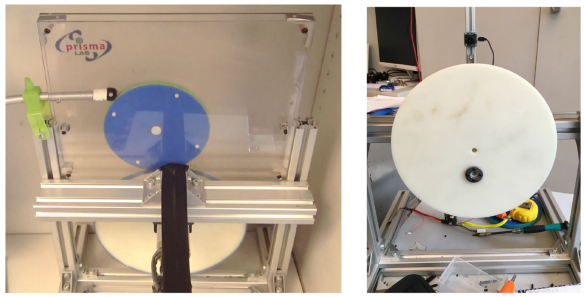

(a) (b)

Fig. 8. Experimental prototype of the eccentric disk-on-disk system. (a) Setup is mounted in full gravity between two plexiglass. Rubber bands of small thickness encircle both disks. On the left, a block allows the possibility to stop the upper disk to set the proper initial condition. (b) Detail of the experimental setup. It is possible to notice the displacement between the geometric center of the disk and its center of rotation attached to the motor shaft (black circle).

The control algorithm, coded in C++, runs on an external PC with a Linux-based operating system. A full-custom 120-W motor driver provides the motor commands. This device can give an accurate measure of the current as feedback, thanks to an ad-hoc designed circuit, while the encoder signal is instead elaborated by a dedicated high-frequency device able to manage the considerable quantity of interrupts of the encoder. The feedback control signals are elaborated by an ARM CORTEX M3 microcontroller (32 bit, 75 MHz), on whose firmware the low-level inner control loop for the current runs at a frequency of 4 kHz. The microcontroller receives the inputs from the external PC through a universal serial bus. The low-level controller outputs the current reference for the motor servo, which provides the torque to the hand. Therefore, the torque u resulting from the IDA-PBC controller is transformed into a current reference, u_c, for the inner-control loop as

$$u_c = \frac{1}{k_m}(u + \mu_d\dot{\theta}_h + f_s\operatorname{sign}(\dot{\theta}_h)) + k_p(\hat{\theta}_h - \theta_h) + k_d(\dot{\hat{\theta}}_h - \dot{\theta}_h) \quad (44)$$

where $\hat{\theta}_h$ and $\dot{\hat{\theta}}_h$ are the desired hand position and velocity, respectively, obtained by integrating the following expression of the hand acceleration, resulting from the dynamics of the eccentric disk-on-disk derived in Section VIII-A:

$$\ddot{\hat{\theta}}_h = \left(\frac{b_{22}}{\Delta}\right)\left(u + \frac{b_{12}h_2}{b_{22}} - h_1\right) \quad (45)$$

where $h_1 = c_{11}\dot{\theta}_h + c_{12}\dot{s}_h + \nabla_{\theta_h}V$ and $h_2 = c_{21}\dot{\theta}_h + c_{22}\dot{s}_h + \nabla_{s_h}V$, while the Coriolis terms are $c_{11} = -\lambda m_o(\rho_h + \rho_o)\dot{s}_h \sin(s_h/\rho_h)/\rho_h$, $c_{12} = -\lambda m_o(\dot{s}_h + \dot{\theta}_h\rho_h)(\rho_h + \rho_o)\sin(s_h/\rho_h)/\rho_h^2$, $c_{21} = \lambda m_o(\rho_h + \rho_o)\dot{\theta}_h \sin(s_h/\rho_h)/\rho_h$, and $c_{22} = 0$. The gains and the parameters in (45) are experimentally tuned as $k_p = 3$, $k_d = 30$, the motor constant $k_m = 0.054$ N·m/A, the viscous friction coefficient $\mu_d = 0.13672$ N·s, and the torque required to overcome friction from rest $f_s = 0.2118$ N·m . The values of μ_d and f_s are found through some preliminary tests as in [11]. The microcontroller executes the computation of u_c at a frequency of 1 kHz.

A visual system provides the measurement of the angular position of the object, $\psi \in \mathbb{R}$, that is the angle that the center of the upper disk forms with respect to Σ_w, increasing

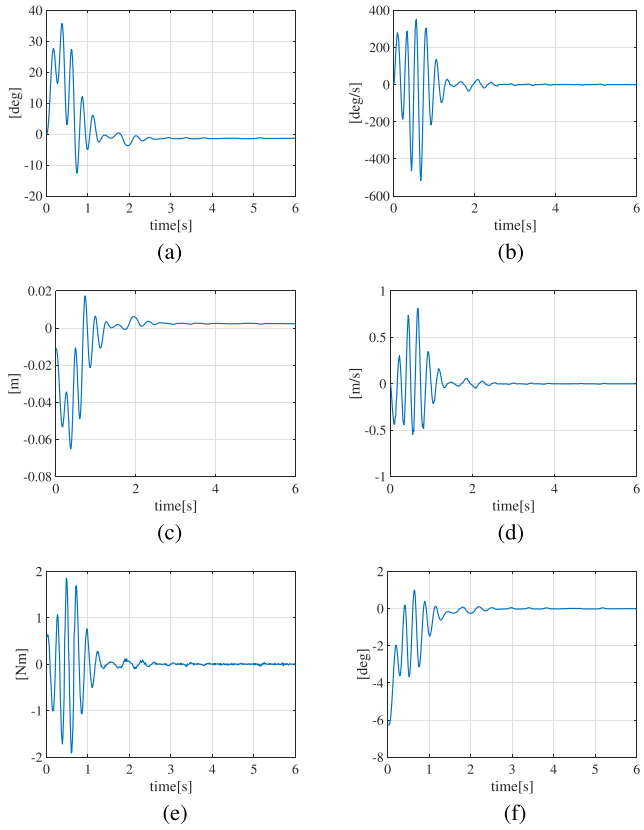

Fig. 9. First experimental test for the eccentric disk-on-disk system controlled by the proposed IDA-PBC controller. (a) Time history of $\theta_h(t)$. (b) Time history of $\dot{\theta}_h(t)$. (c) Time history of $s_h(t)$. (d) Time history of $\dot{s}_h(t)$. (e) Time history of $u(t)$. (f) Time history of $\psi(t)$.

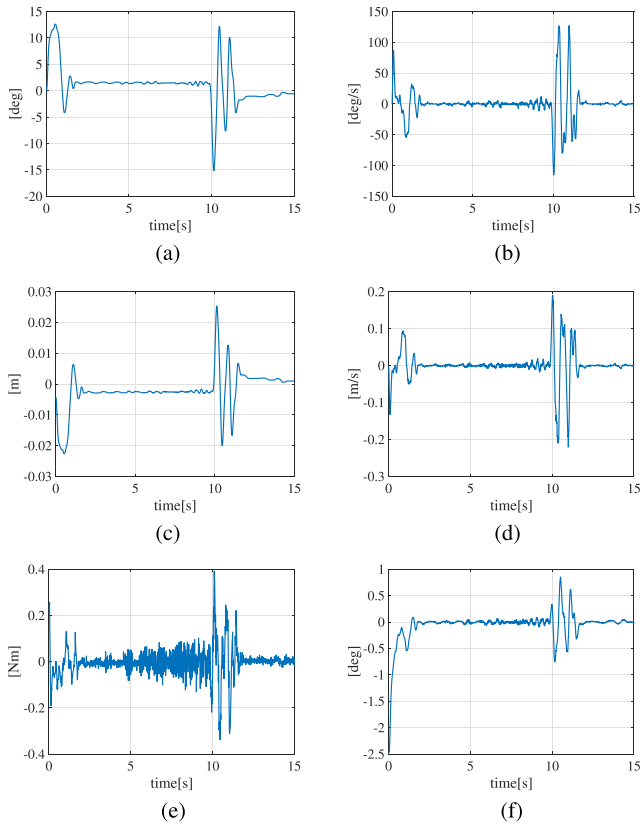

Fig. 10. Second experimental test for the eccentric disk-on-disk system controlled by the proposed IDA-PBC controller. (a) Time history of $\theta_h(t)$. (b) Time history of $\dot{\theta}_h(t)$. (c) Time history of $s_h(t)$. (d) Time history of $\dot{s}_h(t)$. (e) Time history of $u(t)$. (f) Time history of $\psi(t)$.

counterclockwise. This measure is elaborated from the geometry of the system to retrieve the current value of the arclength parameter of the hand: $s_h = \rho_h(\psi - \theta_h - \arcsin\left(\frac{\lambda}{\rho_o+\rho_h}\sin\left(\psi-\theta_h\right)\right))$. The visual system consists of an uEye UI-122-xLE camera providing 360×340 pixel images to the PC at 75 Hz, which is also the high-level controller sample rate to compute u from the IDA-PBC controller. With the aim to increase the efficiency of the vision processing, the image elaboration algorithm focuses on an 80×80 pixel region of interest.

The values of the parameters of the eccentric disk-on-disk dynamic model are $m_o = 0.224$ kg, $m_h = 0.33$ kg, $\rho_o = 0.075$ m, $\rho_h = 0.125$ m, $I_o = m_o\rho_o^2$, $I_h = m_h\rho_h^2$, $\lambda = -0.04$ m, and $g = 9.81$ m/s^2.

In the following, two tests are carried out. The objective is to stabilize the equilibrium $\boldsymbol{q}^\star = (0, 0)$. The controller gains are experimentally tuned as $k = -0.121$, $k_a = 2.05$, $k_v = 0.057$, and $k_f = 3550$. The video of the performed experiments is attached to the manuscript.

Notice that an open question is how generalizing the IDA-PBC approach to set constraints in the contact forces. For this reasons, the friction cones are not explicitly addressed in the formulation. This means that for particular choices of either control gains or initial condition of the system, the upper disk may slip or even lose contact with the lower disk. An analysis would be thus necessary to verify whether the continuous rolling assumption is satisfied during the entire experiments. Such analysis can be performed by empirically measuring the frictional coefficient between the two disks and comparing it with the minimum frictional coefficient necessary to ensure rolling computed from the normal and frictional forces employing the measured experimental data. The procedure is detailed in [1] for the disk-on-disk setup, and it is not reported here, since it is out of the scope from the purposes of this paper.

1) Test 1: In this first test, the chosen initial conditions are $\theta_h(0) = 0$ rad, $\dot{\theta}_h(0) = 0$ rad/s, $s_h(0) = -0.01$ m, and $\dot{s}_h(0) = 0$ m/s. Through these choices, the upper disk starts with an initial angle of about $\psi(0) \simeq -6^\circ$ with respect to the vertical axis of Σ_w.

Fig. 9 shows the results obtained in this first experimental test. In particular, the figure depicts the time histories of $\theta_h(t)$, $\dot{\theta}_h(t)$, $s_h(t)$, $\dot{s}_h(t)$, $u(t)$, and $\psi(t)$. The plots show that the controller can balance the object at the upright unstable position [see Fig. 9(f)], while demanding a sufficiently smooth control torque [see Fig. 9(e)]. However, from Fig. 9(a) and (c), it is possible to notice that θ_h and s_h do not go exactly to zero, respectively, while, instead, the angle ψ does. In particular, the steady-state value of θ_h is around 1.5°, while s_h is around 0.0024 m. These small errors are mainly due to calibration uncertainties of the vision system, plus some uncertainties on the model parameters. These last are rationally related to the experimental identification carried out to estimate the parameters of the motor.

2) Test 2: In this second test, the chosen initial conditions are $\theta_h(0) = 0$ rad, $\dot{\theta}_h(0) = 0$ rad/s, $s_h(0) = -0.0043$ m, and $\dot{s}_h(0) = 0$ m/s. Through these choices, the upper disk starts with an initial angle of about $\psi(0) \simeq -2.5^\circ$ with respect to the vertical axis of Σ_w. The goal is the same as in the first test. Besides, the upper disk is voluntarily perturbed after around 10 s to test the robustness of the proposed control technique against external disturbances.

Fig. 10 shows the results obtained in this second experimental test. As before, the figure depicts the time histories of $\theta_h(t)$, $\dot{\theta}_h(t)$, $s_h(t)$, $\dot{s}_h(t)$, $u(t)$, and $\psi(t)$. The plots show that the controller can balance the object at the upright unstable position [see Fig. 10(f)], while demanding a sufficiently smooth control torque [see Fig. 10(e)], and rejecting an external disturbance. The effects of the external perturbation are easily appreciable from all the plots. As for the first test, from Fig. 10(a) and (c), it is possible to notice that θ_h and s_h do not go exactly to zero, respectively, while, instead, the angle ψ does. In particular, the steady-state value of θ_h is around -0.55°, while s_h is around 0.001 m. The same discussion regarding the source of the small steady-state error expressed in *Test 1* applies also for *Test 2*.

IX. Conclusion

A novel method to reduce the complexity of the IDA-PBC design was proposed in this paper. The achieved results can be applied to any underactuated mechanical systems expressed in the pH form, having a separable Hamiltonian or a nonseparable Hamiltonian indifferently, whose dynamic model has dimension 2. While the proposed approach aims at reducing the design complexity, it preserves the effectiveness of the IDA-PBC method. The proposed procedure employs a target potential energy matching equation, depending on a parameterization of the desired closed-loop mass matrix, to simultaneously simplify the identification of the desired mass matrix and select the desired energy function for the closed-loop system. The control methodology was applied to the class of the nonprehensile planar rolling manipulation systems, overcoming some limitations appearing from a literature review. Two benchmark examples were addressed: the ball-and-beam and the eccentric disk-on-disk case studies. Simulations and experiments on the real physical setup were presented to evaluate the performance of the controllers.

Hence, the described methodology proposes a systematic procedure to design the control law for the broad class of underactuated mechanical planar system through the IDA-PBC framework, without explicitly solving the PDEs of the kinetic matching equation and providing a closed-form solution for the potential matching equation. The introduced design was also a generalization of [20], since it addressed nonseparable Hamiltonian systems without the constraint that the hand must rotate around its CoM: this meant it was thus possible to solve a general nonprehensile planar rolling manipulation problem through the proposed IDA-PBC framework. The chosen benchmark examples highlighted the benefit of employing the described methodology. In particular, it was possible to consider a more complicated, yet accurate, dynamic model for the ball-and-beam example rather than, for instance, in [3] and [14], while neither linearization nor simplification of the dynamic model was needed for the eccentric disk-on-disk example, as in [24] and [25], respectively. Further academic examples that may benefit of the proposed methodology and that are not classifiable as nonprehensile manipulation case studies are the Acrobot and the Pendubot systems, the inertia-wheel pendulum, and the TORA system, with and without gravity.

Future extensions of this paper aim at the development of analytical solutions to remove any potential singularity, which is inherited from the procedure proposed in [19]. Besides, the generalization to systems with higher dimensions than $n = 2$ and $m = 1$ (i.e., three-dimensional (3-D) nonprehensile rolling manipulation systems exhibiting nonholonomic constraints [26]–[29]) is indeed a current work.

Appendix

In this appendix, given $V(q_1, q_2)$, $\alpha(q_1, q_2, \boldsymbol{c}_1)$, and $\boldsymbol{\beta}(q_1, q_2, \boldsymbol{c}_1)$, the explicit solution of (15) is provided for some particular cases. For the sake of clarity, given a generic function $f(a, b, c)$ of its arguments, the function $f(d, e, h)$ is computed by substituting $a = d$, $b = e$, and $c = h$. Some possible cases of interest are reported in the following, but the analysis can be extended.

Case 1: Consider $\alpha(q_1, q_2, \boldsymbol{c}_1) = k_1\gamma(q_1, q_2)$ and $\beta(q_1, q_2, \boldsymbol{c}_1) = k_2\gamma(q_1, q_2)$, with $k_1, k_2 \in \mathbb{R}$ and $\boldsymbol{\gamma}(q_1, q_2) \in \mathbb{R}$ a common function. This case is the one employed in Sections VII and VIII. The explicit solution is

$$V_d(\boldsymbol{q}, \boldsymbol{c}_2) = -\int_1^{q_1} \frac{\nabla_{q_2} V\left(\sigma, \frac{k_1 q_2 - k_2 q_1 + k_2 \sigma}{k_1}\right)}{k_1 \gamma\left(\sigma, \frac{k_1 q_2 - k_2 q_1 + k_2 \sigma}{k_1}\right)} d\sigma + f\left(\frac{k_1 q_2 - k_2 q_1}{k1}, \boldsymbol{c}_2\right) \tag{46}$$

with $f(\cdot) \in \mathbb{R}$ any function of its arguments.

Case 2: Consider $\alpha(q_2, \boldsymbol{c}_1)$, $\beta(q_2, \boldsymbol{c}_1)$, and $V(q_2)$, that is, they depend on the variable q_2 only. The explicit solution for this example is

$$V_d(\boldsymbol{q}, \boldsymbol{c}_2) = -\int_1^{q_2} \frac{1}{\beta(\sigma, \boldsymbol{c}_1)} \frac{dV(\sigma)}{d\sigma} d\sigma + f\left(-q_1 + \int_1^{q_2} \frac{\alpha(\sigma, \boldsymbol{c}_1)}{\beta(\sigma, \boldsymbol{c}_1)} d\sigma, \boldsymbol{c}_2\right). \tag{47}$$

Case 3: Consider $\alpha(q_1, q_2, \boldsymbol{c}_1) = 0$. The explicit solution for this example is

$$V_d(\boldsymbol{q}, \boldsymbol{c}_2) = -\int_1^{q_2} \frac{\nabla_{q_2} V(q_1, \sigma)}{\alpha(q_1, \sigma)} d\sigma + f(q_1, \boldsymbol{c}_2). \tag{48}$$

Case 4: Consider $\beta(q_1, q_2, \boldsymbol{c}_1) = 0$. The explicit solution for this example is

$$V_d(\boldsymbol{q}, \boldsymbol{c}_2) = -\int_1^{q_1} \frac{\nabla_{q_2} V(\sigma, q_2)}{\alpha(\sigma, q_2)} d\sigma + f(q_2, \boldsymbol{c}_2). \tag{49}$$

REFERENCES

[1] A. Donaire, F. Ruggiero, L. R. Buonocore, V. Lippiello, and B. Siciliano, "Passivity-based control for a rolling-balancing system: The nonprehensile disk-on-disk," *IEEE Trans. Control Syst. Technol.*, vol. 25, no. 6, pp. 2135–2142, Nov. 2017.

[2] V. Duindam, A. Macchelli, S. Stramigioli, and H. Bruyninckx, *Modeling and Control of Complex Physical Systems: The Port-Hamiltonian Approach*. New York, NY, USA: Springer, 2009.

[3] F. Gómez-Estern, R. Ortega, F. Rubio, and J. Aracil, "Stabilization of a class of underactuated mechanical systems via total energy shaping," in *Proc. IEEE Conf. Decis. Control*, Orlando, FL, USA, 2001, pp. 1137–1143.

[4] R. Ortega, A. Donaire, and J. G. Romero, "Passivity-based control of mechanical systems," in *Feedback Stabilization of Controlled Dynamical Systems (ser. Lecture Notes in Control and Information Sciences)*, N. Petit, Ed, vol. 473. New York, NY, USA: Springer, 2017, ch. 7, pp. 167–199.

[5] R. Ortega, A. Van Der Schaft , B. Maschke, and G. Escobar, "Interconnection and damping assignment passivity-based control of port-controlled Hamiltonian systems," *Automatica*, vol. 38, no. 4, pp. 585–596, 2002.

[6] J. A. Acosta, R. Ortega, A. Astolfi, and A. M. Mahindrakar, "Interconnection and damping assignment passivity-based control of mechanical systems with underactuation degree one," *IEEE Trans. Autom. Control*, vol. 50, no. 12, pp. 1936–1955, Dec. 2005.

[7] A. Donaire *et al.*, "Shaping the energy of mechanical systems without solving partial differential equations," *IEEE Trans. Autom. Control*, vol. 61, no. 4, pp. 1051–1056, Apr. 2016.

[8] K. Nunna, M. Sassano, and A. Astolfi, "Constructive interconnection and damping assignment for port-controlled Hamiltonian systems," *IEEE Trans. Autom. Control*, vol. 60, no. 9, pp. 2350–2361, Sep. 2015.

[9] D. Prattichizzo and J. Trinkle, "Grasping," in *Springer Handbook of Robotics*, B. Siciliano and O. Khatib, Eds. New York, NY, USA: Springer, 2016, pp. 955–988.

[10] J. Ryu, F. Ruggiero, and K. M. Lynch, "Control of nonprehensile rolling manipulation: Balancing a disk on a disk," in *Proc. IEEE Int. Conf. Robot. Automat.*, St. Paul, MN, USA, 2012, pp. 3232–3237.

[11] J. Ryu, F. Ruggiero, and K. M. Lynch, "Control of nonprehensile rolling manipulation: Balancing a disk on a disk," *IEEE Trans. Robot.*, vol. 29, no. 5, pp. 1152–1161, Oct. 2013.

[12] F. Gordillo, J. Aracil, and F. Gómez-Estern, "Stabilization of autonomous oscillations and the hopf bifurcation in the ball and beam," in *Proc. IEEE Conf. Decis. Control*, Las Vegas, NV, USA, 2002, pp. 3924–3925.

[13] J. Hauser, S. Sastry, and P. Kokotovic, "Nonlinear control via approximate input-output linearization: The ball and beam example," *IEEE Trans. Autom. Control*, vol. 37, no. 3, pp. 392–398, Mar. 1992.

[14] R. Ortega, M. Spong, F. Gómez-Estern, and G. Blankenstein, "Stabilization of a class of underactuated mechanical systems via interconnection and damping assignment," *IEEE Trans. Autom. Control*, vol. 47, no. 8, pp. 1218–1233, Aug. 2002.

[15] K. Ryu and Y. Oh, "Balance control of ball-beam system using redundant manipulator," in *Proc. IEEE Int. Conf. Mechatronics*, Instanbul, Turkey, 2011, pp. 403–408.

[16] M. Cefalo, L. Lanari, and G. Oriolo, "Energy-based control of the butterfly robot," in *Proc. Int. IFAC Symp. Robot Control*, Bologna, Italy, 2006, pp. 1–6.

[17] K. Lynch, N. Shiroma, H. Arai, and K. Tanie, "The roles of shape and motion in dynamic manipulation: The butterfly example," in *Proc. IEEE Int. Conf. Robot. Automat.*, Leuven, Belgium, 1998, pp. 1958–1963.

[18] M. Surov, A. Shiriaev, L. Freidovich, S. Gusev, and L. Paramonov, "Case study in nonprehensile manipulation: Planning perpetual rotations for "Butterfly" robot," in *Proc. IEEE Int. Conf. Robot. Automat.*, Seattle, WA, USA, 2015, pp. 1484–1489.

[19] M. Ryalat and D. Laila, "A simplified IDA–PBC design for underactuated mechanical systems with applications," *Eur. J. Control*, vol. 27, pp. 1–16, 2016.

[20] V. Lippiello, F. Ruggiero, and B. Siciliano, "The effects of shapes in input-state linearization for stabilization of nonprehensile planar rolling dynamic manipulation," *IEEE Robot. Automat. Lett.*, vol. 1, no. 1, pp. 492–499, Jan. 2016.

[21] F. Ruggiero, V. Lippiello, and B. Siciliano, "Nonprehensile dynamic manipulation: A survey," *IEEE Robot. Automat. Lett.*, vol. 3, no. 3, pp. 1711–1718, Jul. 2018.

[22] A. Teel and L. Praly, "Tools for semiglobal stabilization by partial state and output feedback," *SIAM J. Control Optim.*, vol. 33, no. 5, pp. 1443–1488, 1995.

[23] Y. Aoustin and A. M. Formal'skii, "Beam-and-ball system under limited control: Stabilization with large basin of attraction," in *Proc. IEEE Amer. Control Conf.*, St Louis, MO, USA, 2009, pp. 555–560.

[24] Y. Aoustin and A. Formal'sky, "An original circular ball-and-beam system: Stabilization strategy under saturating control with large basin of attraction," in *Proc. Eur. Control Conf.*, Kos, Greece, 2007, pp. 4833–4838.

[25] S. Satpute, R. Mehra, F. Kazi, and N. Singh, "Geometric–PBC approach for control of circular ball and beam system," in *Proc. Int. Symp. Math. Theory Netw. Syst.*, Groningen, The Netherlands, 2014, pp. 1238–1243.

[26] A. Bicchi and A. Marigo, "Dexterous grippers: Putting nonholonomy to work for fine manipulation," *Int. J. Robot. Res.*, vol. 21, nos. 5/6, pp. 427–442, 2002.

[27] V. Duindam and S. Stramigioli, "Modeling the kinematics and dynamics of compliant contact," in *Proc. IEEE Int. Conf. Robot. Automat.*, Taipei, Taiwan, 2003, pp. 4029–4034.

[28] A. Gutiérrez-Giles, F. Ruggiero, V. Lippiello, and B. Siciliano, "Nonprehensile manipulation of an underactuated mechanical system with second-order nonholonomic constraints: The robotic hula-hoop," *IEEE Robot. Automat. Lett.*, vol. 3, no. 2, pp. 1136–1143, Apr. 2018.

[29] K. Lee, G. Batz, and D. Wollherr, "Basketball robot: Ball-on-plate with pure haptic information," in *Proc. IEEE Int. Conf. Robot. Automat.*, Pasadena, CA, USA, 2008, pp. 2410–2415.

Diana Serra received the Ph.D. degree in information technology and electrical engineering from the University of Naples Federico II, Naples, Italy, in 2017.

Her main research interests include passivity-based and optimal control theory applied to mobile and service robotics.

Fabio Ruggiero (S'07–M'10) received the M.Sc. degree in automation engineering and the Ph.D. degree in electrical engineering and information technology from the University of Naples Federico II, Naples, Italy, in 2007 and 2010, respectively.

He was a Visiting Ph.D. Student with Northwestern University from September 2009 to March 2010. After several Postdoctoral positions from 2011 to 2016, he is currently an Assistant Professor of Automatic Control with the University of Naples Federico II. He has coauthored about 50 among journal papers, book chapters, and conference papers. His research interests include dexterous and dual-hand robotic manipulation, even by using unmanned aerial vehicles with small robotic arms, dynamic nonprehensile manipulation, and three-dimensional object preshaping and reconstruction.

Alejandro Donaire (M'13) received the degree in electronic engineering and the Ph.D. degree in system modelling and control engineering from the National University of Rosario, Rosario, Argentina, in 2003 and 2009 respectively.

In 2009, he became a Researcher with the Centre for Complex Dynamic Systems and Control, The University of Newcastle, Callaghan, NSW, Australia, and in 2011, he received the UON Postdoctoral Research Fellowship. In March 2015, he joined the Laboratory of Projects of Robotics for Industry and Services, Mechatronics and Automation, University of Naples Federico II, Naples, Italy, where he worked for two years. In 2017, he joined the Institute for Future Environments, Queensland University of Technology, Brisbane, QLD, Australia, where he was a Senior Research Fellow. Since 2019, he has been with the School of Engineering, The University of Newcastle, and conducts his academic activities within the Mechatronic Discipline. His research interests include nonlinear dynamics, control theory and system design for robotics, mechatronics, and marine and aerospace applications.

Luca Rosario Buonocore received the Ph.D. degree in computer and automation engineering from the University of Naples Federico II, Naples, Italy, in 2015.

He is currently a Research Fellow with the R&D Robotic Division of Engineering Group, European Organization for Nuclear Research, Genève, Switzerland. His main research interests include mechatronic design of novel robotic solutions, such as mobile robotic platforms and ultralight robotic arms for areal manipulation.

Vincenzo Lippiello (SM'17) was born in Naples, Italy, in 1975. He received the Laurea degree in electronic engineering and the Research Doctorate degree in information engineering from the University of Naples Federico II, Naples, in 2000 and 2004, respectively.

He is currently an Associate Professor of Automatic Control with the Department of Electrical Engineering and Information Technology, University of Naples Federico II. He has authored or coauthored more than 120 journal and conference papers and book chapters. His research interests include visual servoing of robot manipulators, hybrid visual/force control, adaptive control, grasping and manipulation, aerial robotics, and visual object tracking and reconstruction.

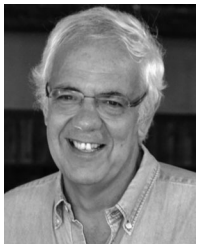

Bruno Siciliano (M'91–SM'94–F'00) was born in Naples, Italy, in 1959. He received the Laurea and Research Doctorate degrees in electronic engineering from the University of Naples, Naples, in 1982 and 1987, respectively.

He is currently Professor of Control and Robotics and Coordinator of PRISMA Lab with the Department of Electrical Engineering and Information Technology, and Director of the Interdepartmental Center for Advances in Robotic Surgery and the Coordinator of the Laboratory of Projects of Robotics for Industry and Services, Mechatronics and Automation, University of Naples Federico II, Naples, Italy. He has delivered more than 150 keynotes and has authored or coauthored more than 300 papers and seven books.

Mr. Siciliano is a Fellow of the American Society of Mechanical Engineers and the International Federation of Automatic Control. He is a recipient of numerous international prizes and awards. He was the President of the IEEE Robotics and Automation Society from 2008 to 2009. Since 2012, he has been on the Board of Directors of the European Robotics Association. His book "Robotics" is among the most adopted academic texts worldwide, while his edited volume *Springer Handbook of Robotics* received the highest recognition for scientific publishing: 2008 PROSE Award for Excellence in Physical Sciences & Mathematics. His research team got 16 projects funded by the European Union for a total grant of Million Euro in the last ten years, including an Advanced Grant from the European Research Council.